12-2016

In-situ particle sizing of agglomerates in aluminized solid composite propellants using digital inline holography (DIH)

Michael S. Powell
Purdue University

Graduate School Form
30 Updated 12/26/2015

PURDUE UNIVERSITY
GRADUATE SCHOOL
Thesis/Dissertation Acceptance

This is to certify that the thesis/dissertation prepared

By Michael Stephan Powell

Entitled

IN-SITU PARTICLE SIZING OF AGGLOMERATES IN ALUMINIZED SOLID COMPOSITE PROPELLANTS USING DIGITAL INLINE HOLOGRAPHY (DIH)

For the degree of Master of Science in Mechanical Engineering

Is approved by the final examining committee:

Steven Son
Chair

Ibrahim Emre Gunduz

Jun Chen

To the best of my knowledge and as understood by the student in the Thesis/Dissertation Agreement, Publication Delay, and Certification Disclaimer (Graduate School Form 32), this thesis/dissertation adheres to the provisions of Purdue University's "Policy of Integrity in Research" and the use of copyright material.

Approved by Major Professor(s): Steven Son

Approved by: Jay Gore 11/30/2016

Head of the Departmental Graduate Program Date

IN-SITU PARTICLE SIZING OF AGGLOMERATES IN ALUMINIZED SOLID COMPOSITE PROPELLANTS USING DIGITAL INLINE HOLOGRAPHY (DIH)

A Thesis

Submitted to the Faculty

of

Purdue University

by

Michael S. Powell

In Partial Fulfillment of the

Requirements for the Degree

of

Masters of Science in Mechanical Engineering

December 2016

Purdue University

West Lafayette, Indiana

This thesis is dedicated to Neva for all of her love and support through my graduate studies.

ACKNOWLEDGEMENTS

I would like to thank everyone in the lab for all of the help over the years. Brandon, Sarah, Andrew, Luciano, Omar, and Hatem. I would also like to thank Dr. Gunduz and Dr. Guildenbecher for their help with experiments and data analysis. Without them, this project would have been far less feasible.

This material is based upon work supported by the AFOSR MURI contract FA9550-13-004 with Mitat Birkan as Program Manager.

TABLE OF CONTENTS

Page

LIST OF TABLES

Table Page

LIST OF FIGURES

Figure Page

ABSTRACT

Powell, Michael S. MSME, Purdue University, December 2016. In-Situ Particle Sizing of Agglomerates in Aluminized Solid Composite Propellants Using Digital Inline Holography (DIH). Major Professor: Steven S. Son, School of Mechanical Engineering

Aluminized ammonium perchlorate composite propellants (APCP) form large molten agglomerated particles that can result in poor combustion performance and increased two-phase flow losses. Quantifying agglomerate size distributions is important for assessing these losses for different types of aluminum fuels that can help improve rocket performance. It is highly desirable to measure particle sizes *in-situ* using non-intrusive optical methods, rather than conventional particle collection, which can have large uncertainties. Regular high-speed microscopic imaging suffers from a limited depth of field. Digital inline holography (DIH) is an alternative approach that results in 3D information through numerical reconstruction. In this paper, DIH approach was used with two orthogonal viewing angles for simultaneous particle imaging and velocity measurements. Furthermore, two imaging speeds (4 Hz vs. 4,000 Hz) were compared to characterize biasing. DIH results were contrasted with high-speed visual imaging and conventional particle collection. All techniques were in agreement that ejected particles were larger than initial constituent particles. However, DIH allows for the acquisition of much less experimental data for statistically significant data sets when compared to videography and more accurately sizes agglomerates than particle collection. Low-speed

DIH is found to be subject to biasing due to multiple counting of larger particles with slower velocities staying in the field of view. A model was employed to correct the velocity biasing was performed by adjusting the data based on size and velocity correlations. This was partially successful to reduce biasing of sizes for the low speed DIH data.

1 INTRODUCTION

Aluminum has been used as a fuel additive in rocket propellants since the 1950's. Its use as a fuel is widespread from large scale solid rocket boosters to hobbyist rocket motors. Aluminum powder raises the specific impulse (I_{sp}) through the product molecular weights and increased flame temperature [1]. It also suppresses high-frequency combustion instabilities through viscous particle damping [2]. The use of aluminum powder in propellant comes with self-induced efficiency reduction in the form of two phase flow losses.

Aluminized ammonium perchlorate composite propellants (APCPs) form large molten aluminum (Al) agglomerates leading to incomplete combustion and two-phase flow losses [3-5]. These large molten droplets (LMD) form from the coalescence of multiple Al particles and they are often an order of magnitude larger than the initial constituent particle size [4,6]. The momentum and thermal dis-equilibrium between the condensed and gaseous products, collectively known as two-phase flow losses, are more significant for larger particles [7,8], especially compared to smaller particles like nanoaluminum [9-13]. However, nAl has a higher cost, typically contains a large amount of oxide (>20wt.%), and results in poor rheology of the propellant grains due to the high specific surface area [6,10,13]. In addition to two-phase flow losses, slag build up in the rocket exhaust, resulting from the impinging of these molten alumina particles, is of concern

because of its extra weight, among other undesirable effects [14]. Shown in Fig. 1 is an example of an Al LMD burning in-situ.

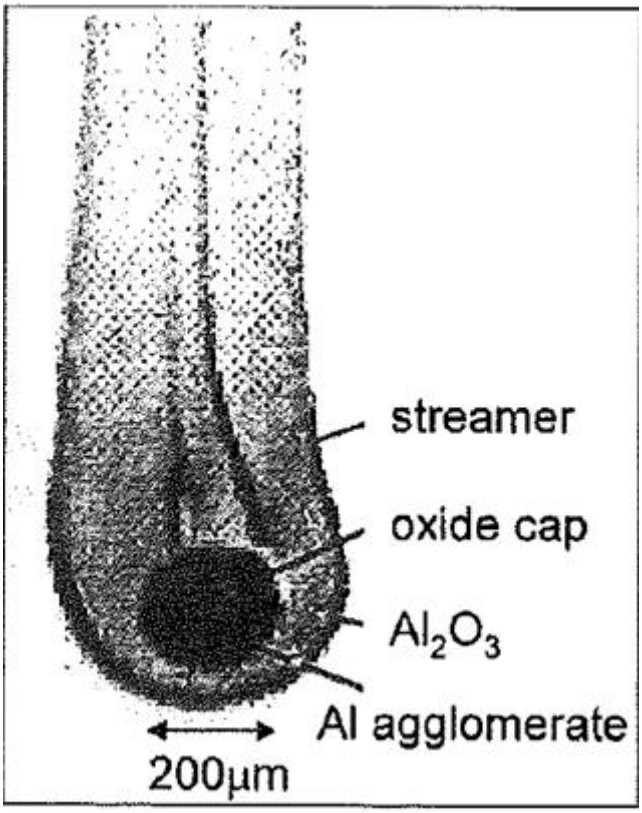

Fig. 1. An aluminum LMD burning. Initial particle size of aluminum additive was 5 μm [1].

The mechanisms of aluminum agglomeration and combustion has studied before to understand the particle dynamics and phenomena in the gas phase [1,4,5,6,7,13,15,16,17]. Agglomeration reduction would lead to a reduction in two phase flow losses, slag reduction, and less nozzle erosion. Characterization techniques for sizing agglomeration and mechanisms for aluminized APCPs would lead to rapid and accurate determination of agglomeration for novel propellant formulations. Currently, techniques for sizing Al agglomerations in APCPs include phase doppler anemometry [18], laser diffraction [19],

particle collection [4,6,13,19], videography [1,4,20], schlieren [21], shadowgraphy [20], holography [22-25], and digital inline holography (DIH) [26]. The primary methods of interest are optical techniques as the dynamics of the system are not perturbed.

1.1 Videography

Videography using microscopic lenses has also been used for imaging Al agglomerates to size LMDs, and as with particle collection, a non-trivial amount of agglomerates was found to be much larger than the initial Al particle size [4,20,27]. Favorably, this technique does not affect the propellant flames or interfere with the droplet burning process and surface phenomena and agglomerates could be viewed in-situ. Emission spectra from burning aluminum is broadband from infrared to ultraviolet [28,29]. Oversaturation of any camera system is of concern for this reason. Shown in Fig. 2 is an oversaturated image from an experiment using the technique of videography and the proposed agglomeration mechanism. Exposure time, filters, backlighting, and apertures can be used to adjust the incoming light to size particles. In order to distinguish between the smoke of a particle burning, and a liquid particle an Abel transformation must be used [27]. After transformation, particles can be measured for agglomeration sizing. Only particles that are in the narrow focal plane can be imaged and sized accurately using this technique, so each video frame provides only a few particles. This requires larger amounts of recordings to get a statistically significant data set.

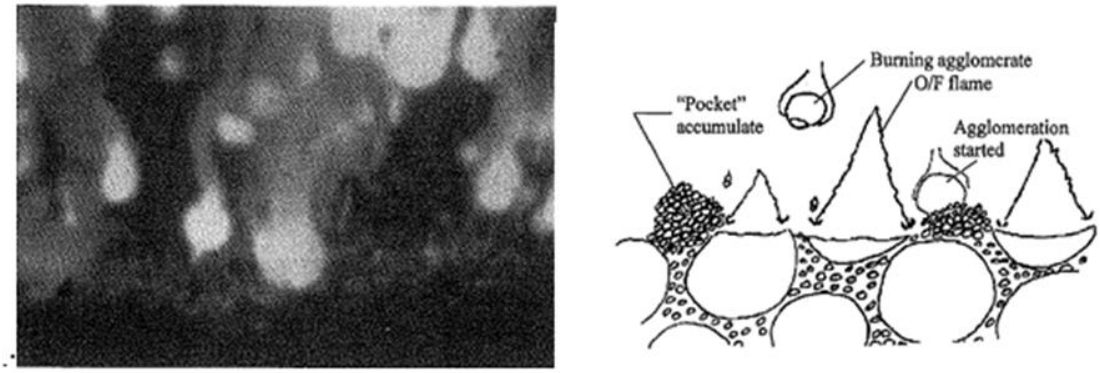

Fig. 2. Left, an image of the agglomeration process. Overexposure of the camera causes the LMD to appear white. Right, a diagram of the proposed agglomeration mechanism [4].

1.2 Particle Collection

Particle collection is an intrusive measurement technique for gathering samples to be used for sizing LMD. Particle collection can be performed at high pressure, where optical based techniques have difficulty illuminating the samples. A drawback to this technique is the lack of recording in-situ flame events. Particles have been quenched and collected using either solid and liquid media [6,13,17,18,19]. LMD can be collected are various points in the flow; however, the most relevant is larger agglomerates ejected near the surface of the propellant. As collection probes are moved downstream, LMD sizes decrease as particle burn times are increased [19]. A decrease in LMD size closer to surface of the propellant will reduce nozzle erosion in a motor geometry as agglomerates will be smaller downstream and reduce two phase flow losses. Agglomerates were found to be an order of magnitude or larger than initial constituents [6,13,14].

Particles that are quenched using the particle collection technique are subject to becoming oblate due to the rapid decrease in momentum from impacting the quenching probe or media. This will lead to a bias in the calculated diameter towards larger diameters

using this technique for sizing particles. Little has been reported in literature about the characterization of the amount of flattening of LMD impacting quench probes. A large number of particles can be collected from one experiment. Statistics for LMD sizes can be achieved with little material [30].

1.3 Digital Inline Holography (DIH)

Holographic techniques have also been applied to propellant combustion to record holograms of Al agglomerations [22-26]. Briefly, holography utilizes the interference between two light waves to record a light field which can be reconstructed to produce a 3D hologram [31]. As with other techniques, a significant portion of agglomerates were found to be larger than initial constituents, but there was noteworthy obfuscation from alumina smoke when recording holograms at higher pressures [24,25]. Reconstruction of plumes allowed for a greater number of particles to be viewed and sized from one image when compared to videography. Recorded holograms were originally imaged onto plates, leading to only one hologram per experiment. Smaller particles may have also been missed due to the limitations of the laser and the film media used [22,24]. Multiple holograms can be recorded per experiment through digital recording. Recently, camera repetition rates are what limit the number of holograms that can be recorded in DIH, as with recording holograms of LMD [26].

Fig. 3. depicts the recording process for digital in-line holography (DIH). A planar wave of light is sent through a volumetric field through the section of interest into an imaging device. Traditionally, two lasers pulses are needed to produce a hologram with a reference leg and the diffraction beam (test section leg). Coherence between the reference

leg and the diffracted beam produces a hologram [22,32]. Resolution of the hologram is dependent on the CMOS camera used and the wavelength of the beam used [32,33]. Smaller wavelengths produce smaller diffraction patterns around objects [32,34]

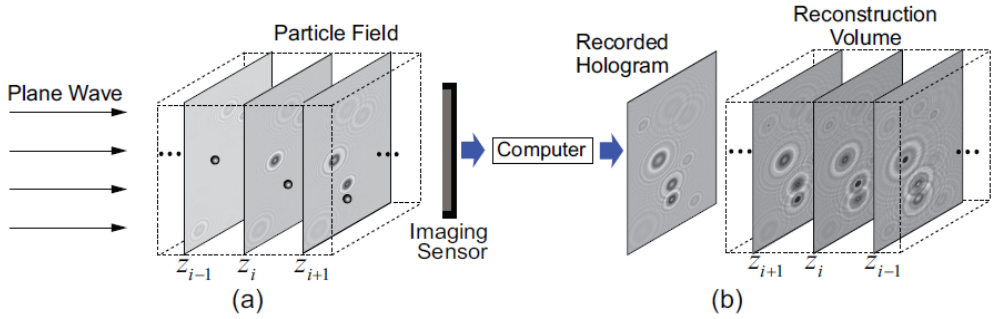

Fig. 3. Depiction of DIH, for recording (a), and reconstruction (b) **[33]**.

An inline configuration can be used to decrease the difficulty in imaging and recording of the hologram, assuming the wavelength is small enough to diffract around objects. This has been demonstrated in previous experiments [26,33]. Eqn. 1 demonstrates how a hologram is made [33,35]

$$E(x,y;z) = [I_0(x,y)E_r^*(x,y)] \otimes g(x,y,z) \tag{1}$$

E is the reconstructed amplitude of the incoming laser light, $I_0(x,y)$ is the intensity of the recorded light of the hologram with respect to the planar wave (x,y), E^*_r is the reference wave light (non-reflected laser light), $\otimes$ is the convolution operation and $g(x,y,z)$ is the Reyleigh-Sommerfield diffraction kernel which can be expressed as shown in Eqn. 2 [33]

$$g(x,y;z) = {e^{jk\sqrt{x^2+y^2+z^2}}}\Big/{j\lambda\sqrt{x^2+y^2+z^2}} \tag{2}$$

Here z is the propagation distance, or reconstruction distance, λ is the wavelength of the incoming laser light (532 nm), and k is the wave number (18,796.99 cm^{-1} for 532 nm wavelength light). In order to resolve Equation (1) and (2), a numerical solution is required, which involves the Fourier transform of Equation (1). Shown below in Equation (3) is the numerical reconstruction equation for reconstructing an image. F is the Fourier transform and F^{-1} is the inverse Fourier transform, and G is the Fourier transform of Equation (2), as shown by Equation (4), and f_x and f_y are respectively the spatial frequencies in their respective directions [33].

$$E(x,y;z) = F^{-1}\{F\{I_0(x,y)\} * G(x,y,z) \tag{3}$$

$$G(x,y;z) = \exp\left(jkz\left(1-\lambda^2 f_x^2 - \lambda^2 f_y^2\right)\right) \tag{4}$$

A focal volume can be imaged in an experiment. Images planes can be reconstructed leading to many more particles that can be analyzed per image (hologram) recorded. Gas phase phenomena can also be observed using this technique. Minimization of material would aid in reducing experimental costs for new propellant formulations. Data analysis for sizing agglomerates is also simplified as labor is shifted to computational methods to size particles.

Improved characterization techniques for determining agglomerate sizes and associated mechanisms for aluminized APCPs could lead to rapid and accurate evaluation of novel propellant formulations. The objective of this work is to further explore and validate DIH as a method of sizing Al agglomerates in dynamic combustion environments. In order to justify the accuracy of DIH, it will be simultaneously compared to established techniques

of particle sizing and videography applied to the same propellant formulations under atmospheric conditions. DIH will also be compared to itself via a transverse high speed view to estimate the biasing of velocity of particles on sizing agglomerations. A model developed will be used to correct the low speed DIH results.

2 EXPERIMENTAL METHODS

Two propellant formulations were used for experiments prepared using the same method reported in previous work [6,13]. One propellant consisted of spherical (Valimet H30), while the other used flake Al (Poudres Hermillon YX-49). Each of the powders were sieved between -200 and +500 mesh sieves to the size range of 25-75 μm. A bimodal distribution of ammonium perchlorate (AP) was used consisting of 71% of the total propellant weight with a 4:1 coarse to fine ratio, with average AP diameters of 200 μm and 20 μm (ATK) respectively. The remaining 15% of the solid loading by weight was aluminum powder (flake or spherical), resulting in a solids loading of 86%. Binder consisted of 10.53% R45M hydroxyl-terminated polybutadiene (Firefox Enterprises), 0.20% Tepanol HX-878 (3M Corp.), 2.11% isodecyl pelargonate (RCS RMC), and 1.16% isophorone diisocyanate (Firefox Enterprises) of the total propellant weight. Components were mixed in stages, initially by hand, for 5 minute intervals and then with a LabRAM resonant mixer (Resodyn) operated at 90% intensity for 5 minutes. Samples were held at a vacuum <35 mbar for 10 minutes to remove air bubbles. Propellant was then packed into 6.75 mm diameter strands measuring ~60 mm in length. Strands were cured in a convection oven at 60 °C for seven days. Shown in Table 1 are the formulations utilized in this work.

Table 1. Mass of materials used to make propellants.

Additive	Total Mass Percentage (%)	Mass [g]
HTPB	10.53%	22.65
Tepanol	0.20%	0.43
IDP	2.11%	4.53
IPDI	1.16%	2.49
Aluminum Additive	15.00%	32.25
Coarse AP (200 μm)	56.80%	122.12
Fine AP (20 μm)	14.20%	30.53

A Vision Research Phantom 7.3 high speed camera was operated at 5000 fps at 1 μs exposure with a window of 400 x 300 pixels for recording ~1.5 sec of video. A long distance microscope (Infinity K2) with a CF2 objective was used with the camera. The internal aperture of the K2 lens was set at the minimum opening to cut down the intense broadband emission from burning LMD and to increase depth of field. A focused green light emitting diode (LED) was used for backlighting to contrast the background from the dense product particles. A 532 nm optical notch filter with 20 nm FWHM was used to reduce broadband emission from Al particles, while allowing most of the light from the green LED. Experimental apparatus is depicted in Fig. 4. Spatial resolution was measured to be ~5.49 μm/pixel when the sample was at the shortest working distance allowed by the lens (~50 mm). Propellant samples were sectioned to 15 mm in length for these experiments. Particle sizes were analyzed using a Matlab code that uses built-in edge detection algorithms.

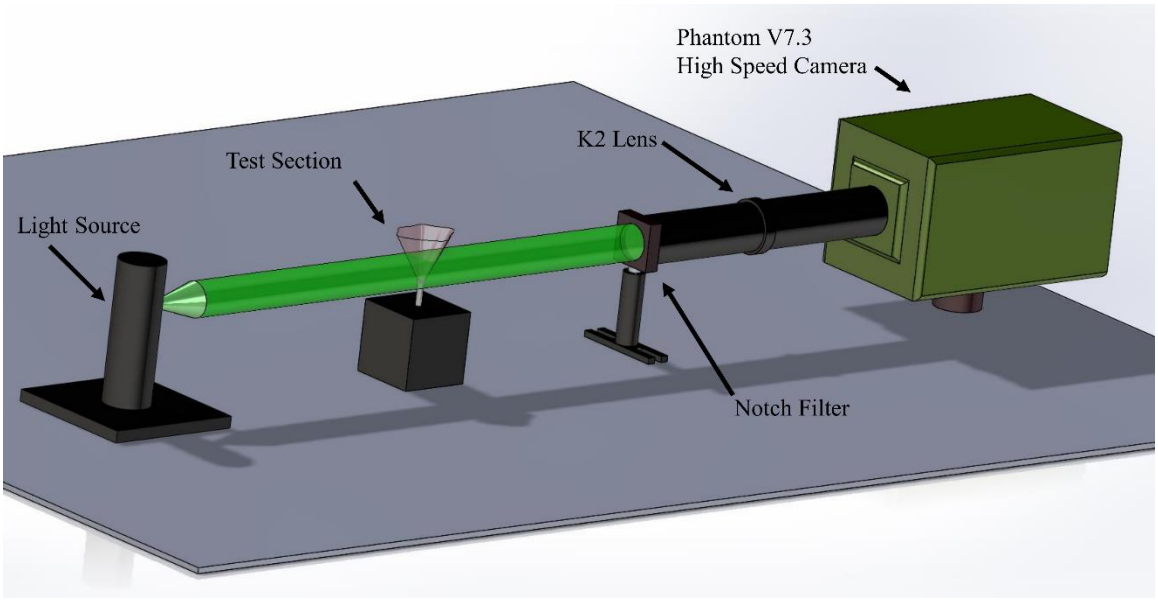

Fig. 4. Apparatus used for videography experiments. Coherent light with a narrow linewidth was used as a backlight. An optical notch filter was used to cut down on the intense light emission from burning aluminum particles.

Particle collection was performed using an apparatus reported previously that was used for high pressure experiments inside of a combustion vessel, as can be seen in Fig. 5 [6,13]. The setup was modified to work in open atmosphere in order to compare to the other techniques listed. Strands of propellant about 15mm in length were ignited using a nichrome wire. A propellant sample was used as a beam block for a 10 mW helium-neon laser until the burning surface recessed below the laser level. Impingement of the laser onto a photo diode triggered a circuit to reverse the polarity of a DC motor allowing a collection plate to swing through the propellant plume and collect quenched particles. Particles were collected at a height ~2-6 mm above the propellant surface at a transverse speed of ~7 m/s onto borosilicate quench disks (McMaster Carr 8477K18). The samples were then imaged using a MX (G)-10C lens on a Hirox digital microscope with an OL-140 II adapter. Using this lens and adapter combination a pixel pitch of ~1.4 μm/pixel can be achieved. In order to size particles, a binary contrast of the image was produced using

ImageJ to outline particles for 2D sizing via the area occupied by the particle in the image. Particle selection was automated using ImageJ as particles can be outlined via selection by color and contrast from the raw image. These areas measured were converted to an equivalent circular area. Number and volumetric diameters and distributions were calculated with respect to the equivalent circular area diameter.

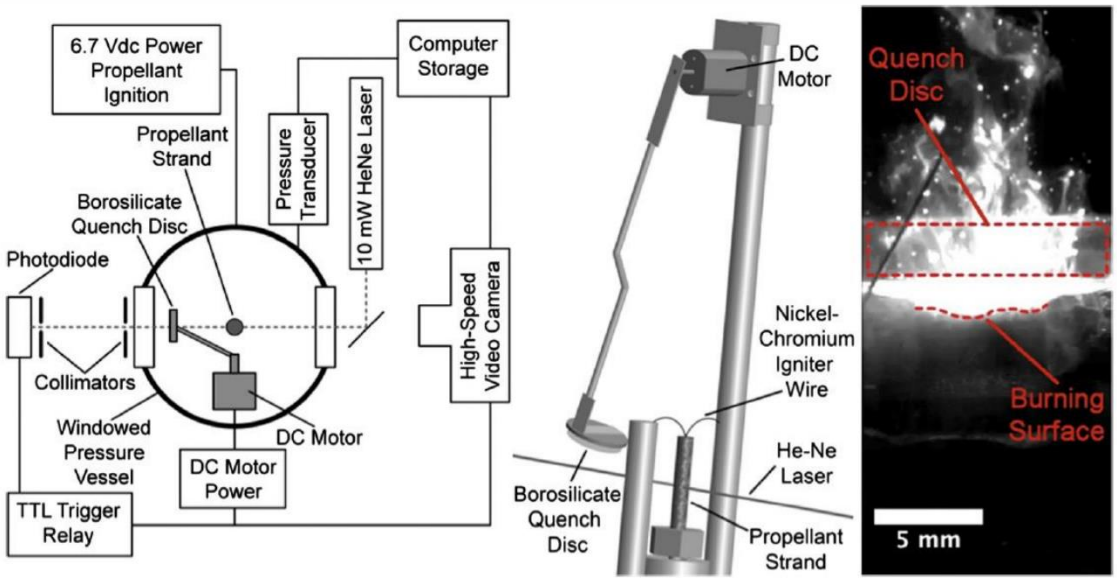

Fig. 5. Apparatus used for particle collection. Apparatus was lightly modified to work outside of a pressure vessel. A laser beam was used to trigger a photodiode to reverse the polarity of the DC motor to swing the quench plate.

The equipment used for DIH is similar to the apparatus used in previous work [26]. Notably, this work focused on a new aspect of DIH, specifically perpendicularly offset adjacent views. One view had a low repetition rate with a large field of view while the view transverse had a fast repetition rate with a limited field of view. The field of views, pixel pitches, and frame rates were 4000 x 2700 and 800 x 600 square pixels, ~1.9 μm/pixel and ~7.9 μm/pixel, and 4 Hz and 4,000 Hz respectively. A double pulsed 532 nm Nd:YAG laser (New Wave Solo PIV laser) was implemented as the illumination source for the low

speed view, while a low powered continuous wave Nd:YAG laser was implemented for the high speed view. The ~3 mm diameter beam for both views was spatially filtered prior to expansion. The final diameter of the beam was 50 mm. A 532 nm notch filter with +/- 1.0 nm FWHM was utilized to block extraneous light from the burning propellant. Figure 6 is a sketch of the apparatus used for recording high speed and low speed holograms. Particle velocities were measured using the high speed view. Reconstruction of holograms, sizing, and velocity measurements were completed autonomously at Sandia National Laboratories, in a similar analysis reported previously [36].

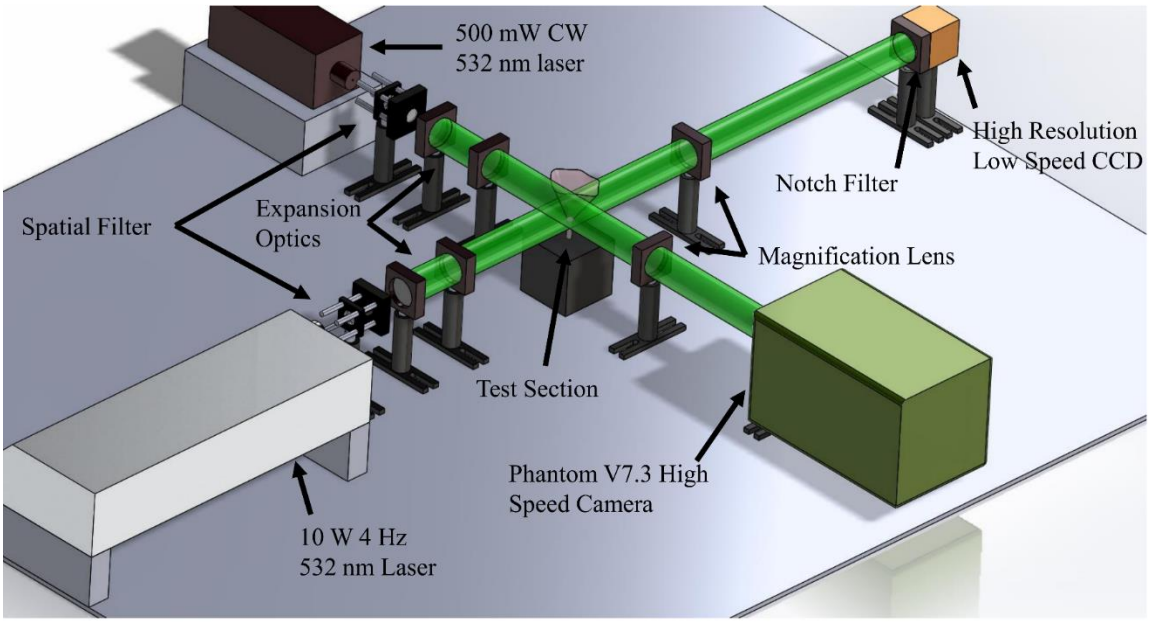

Fig. 6. Setup for the transverse DIH experiment. The high speed view was perpendicular to the low speed view. 4 Hz laser output was limited to ~1 W of power to prevent damage to the camera.

.

3 RESULTS AND DISCUSSION

Al agglomeration occurs due in large part to the difference in the ignition temperature and melting temperature of Al particles [7, 4, 1]. Before ignition, multiple Al particles tend to melt and coalesce on the surface of the propellant from heat conduction from the propellant flame, forming larger spherical droplets due to surface tension. Binder and AP decomposition evolve gases that induce drag forces on the molten droplet, which eventually gets ejected from the propellant surface. This mechanism is shown in Fig. 7. Sometimes these agglomerates can form long chains from the surface of the propellant, as shown in Fig. 2 [6].

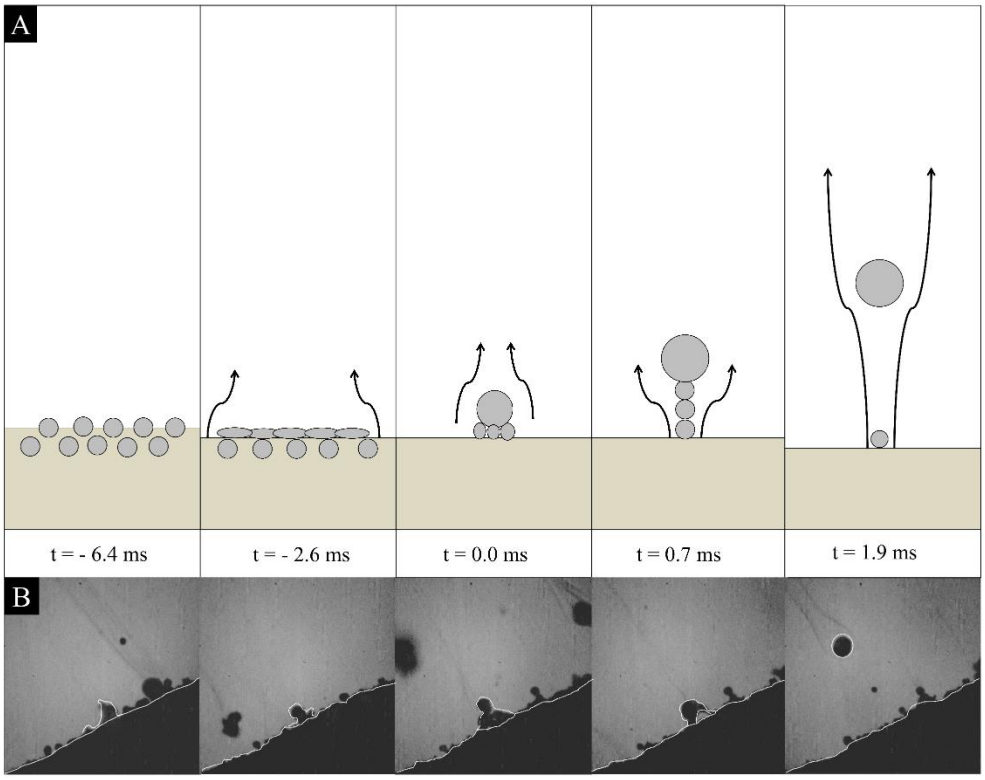

Fig. 7. [A] Agglomeration mechanism for aluminized propellants. Particles melt, coalesce, and eventually lift off due to surface gas generation, or can follow a chain mechanism [6]. [B] In-situ still images of the agglomeration process. Outlined is the surface of the propellant and coalescence of Al droplets.

Representative images showing particle detection for each technique are shown in Fig. 3. Demonstrated in the top row of Fig. 8 is the process of particle selection for particle collection. Image A is the raw collection plate image while image B is the binary contrast of that image for the baseline aluminized propellant. Quenched products for flake Al using particle collection is similar to baseline Al, but with noticeably larger agglomerates present on the quench disk. Detection of LMD for particle collection requires high contrast to distinguish between the collection surface and agglomerates. Depending on the relative contrast of the images, most image processing software is capable of isolating the particles

from the background. Here we used ImageJ for particle collection and Matlab for videography and DIH. Based on the area encircled by the outline of the particle, a diameter from an equivalent 2D circular area was calculated. A concern for this type of particle collection is droplet "splatter" that may bias results towards larger agglomerates; however, the collected particles do not appear to be excessively flattened.

Videography, shown in image C in Fig. 8, utilizes a similar approach to calculating particle diameters as particle collection. Edge detection is accomplished using a Sobel filter. The measured area is then used to calculate a diameter from an equivalent circular area. Not all particles in view were tracked due to lower edge contrast for particles that were not in focus. Numerically, the number of particles that can be imaged for sizing by videography is limited as particles that are in the focal plane are the only particles that can be measured accurately. Over-estimation of particle sizes is less likely to occur with videography as particles are not subject to flattening, unlike with particle collection where particles with higher velocity are more subject to splatter.

Image D of Fig. 8 shows a result of low speed DIH imaging for a baseline aluminized propellant. Highlighted are individual reconstructed focused particle planes superimposed onto the same image. Numerical image reconstruction yields many image planes for sizing LMDs. The diameters can be calculated from the area of the particles, just as with the other techniques. Particle size biasing is reduced in this technique as the measurement does not perturb LMD as with particle collection. DIH has the advantage of producing many more particles that can be sized from one image over videography, as many focal planes are accessible.

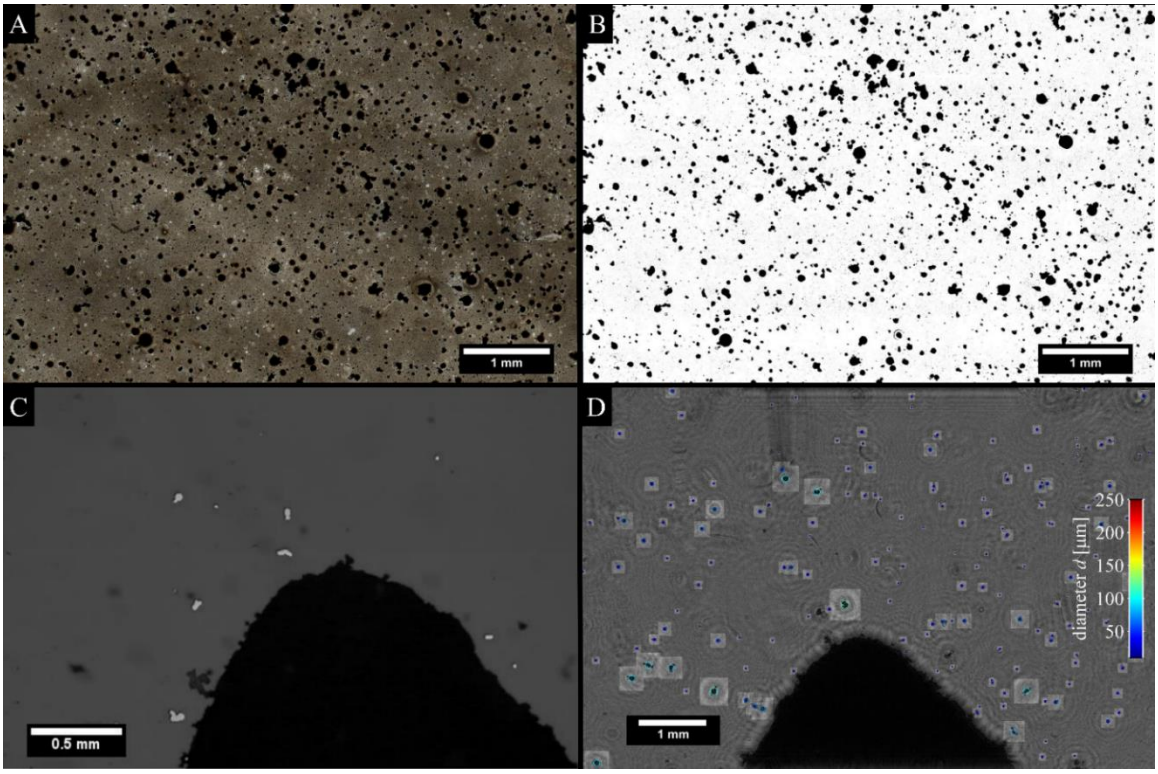

Fig. 8. [A, B] High resolution imaging of particle quench disk. Left image is the raw image from an experiment, while right is a binary contrast of the image for particle sizing. [C Still image taken from a backlit video. Tracked particles that are in focus are highlighted in white. [D] DIH results superimposed onto the same image. Size of the particle diameter is highlighted surrounding the particle, and given as a color intensity.

Droplet sizes can be compared using all three techniques through number and volumetric probability density function (PDF). Raw counts are binned logarithmically to have equal bin sizes in a lognormal plot. Number PDFs follow,

$$q_0 = \frac{q}{\sum q * \Delta x} \tag{5}$$

while volumetric PDFs are of the form,

$$q_3 = \frac{q * x^3}{\sum q * x^3 * \Delta x} \tag{6}$$

where q is defined as the raw count of particles, q_0 is the numerical PDF, q_3 is the volumetric PDF, x is the diameter, and Δx is the bin width (logarithmic scale). Fig. 9 shows the results of particle collection, videography, and low-speed DIH compared to each other using these PDFs. The D_{10}, D_{50}, and D_{90}, (10%, 50%, and 90% of the diameter volume weighted respectively), for each material are also shown. The total number of analyzed particles were 10,000, 1,000 and 20,000 for particle collection, videography, and for DIH respectively. Twenty logarithmically distributed bin sizes are used to demonstrate orders of magnitude differences between bins, and sizes of agglomerates.

All three techniques show agreement that the flake LMD are significantly larger than the spherical baseline propellant based on all three diameter calculations (D_{10}, D_{50}, and D_{90}). Likewise, the volumetric PDF maximum values are shifted towards larger diameters for the flake Al based propellant compared to the spherical baseline propellant. Smaller LMDs are of a relatively high count across all techniques with maximum values near 10-20 μm for both propellant formulations; however, a majority of the mass or volume is concentrated in larger particles as shown by the central peaks for the volumetric diameter being close to or above 100 μm. Spherical Al shows a D_{50} peak near 100 μm for particle collection and low-speed DIH both of which are larger than initial constituent particles for spherical Al that have a D_{50} of 43.3 μm [6,13]. The increase in particle size mass for ejected particles could lead to increased two-phase flow losses. Videography results show a peak in D_{50} of ~59 μm for spherical baseline and is smaller when compared to both particle collection and DIH, which is of similar order to the initial constituent size D_{50} for spherical baseline aluminum. There were also no particles detected above 200 μm for videography

leading to a shift towards smaller particles. This is in disagreement between particle collection and low-speed DIH where particles were found to be even greater than 200 μm.

Similarly, the flake Al produced D_{50} larger than initial constituent particles with a D_{50} of ~230 μm. Across all three techniques, flake Al D_{50} was found to be much larger than spherical baseline. Volumetrically weighted, flake agglomerate diameters are almost twice as large when compared to spherical Al. Similar trends in volumetric and number PDF were found before with particle collection [6,13]. All three techniques are consistent with D_{50} LMD being much larger than initial Al sizes and approximately agree with each other. Similarly, with spherical baseline, the diameters reported using videography are smaller for flake Al than with the other techniques.

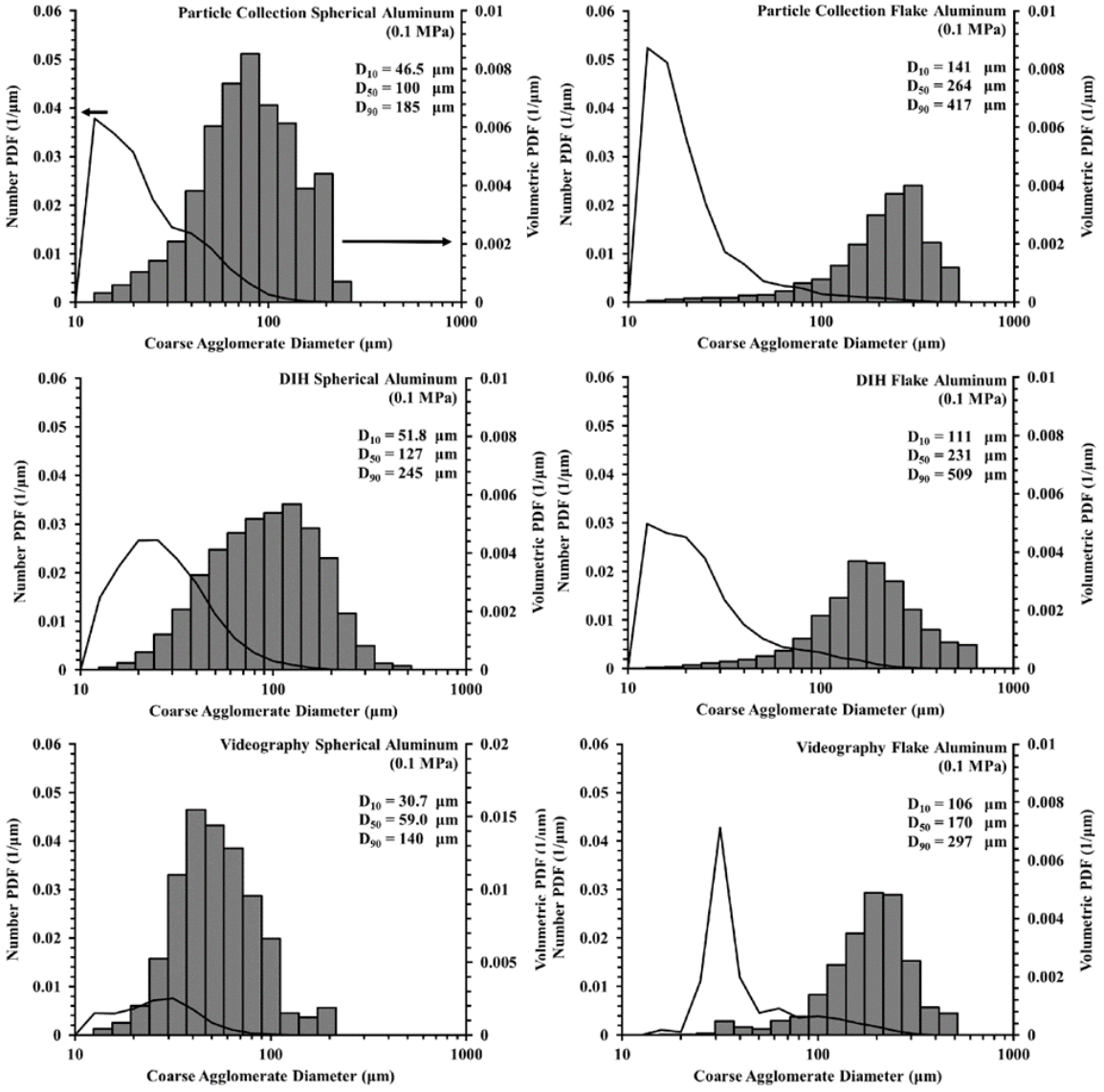

Fig. 9. Size comparisons for all three techniques presented in this paper. Lines indicate number PDF while bars indicate volumetric PDF. The left hand column represents spherical baseline aluminized propellants, while the right hand column corresponds to flake Al. In order from top to bottom is particle collection, low speed DIH, and videography results.

Low-speed DIH was also compared to itself using a high-speed adjacent perpendicular view. Shown in Fig. 10 is the comparison of high speed to the low speed particle tracking and sizing from transverse views. Volumetric diameters for low-speed DIH are larger for both spherical and flake geometries when compared to high speed

results. Largest LMD diameters are where the greatest discrepancy occurs for the dual view DIH, especially for flake Al, where diameter differences for D_{90} is close to a factor of two between the two techniques. It should also be noted that high-speed DIH results are very close to the videography results comparing diameters and distributions in Figs. 4 and 5. One proposed reason for this may be that larger, slower moving LMDs are being counted multiple times in the low-speed DIH. Bias correction for this analysis can be performed based on the measured velocities for different particle diameters. To accomplish this, a fitting function in the following power law form was formulated,

$$v_x = x_1 - x_2 * d^{x_3} \tag{7}$$

where v_x is the velocity in the axial direction, d is the diameter, and $x_{1,2,3}$ are fitting factors. In order to offset the effect of multiple counting of particles from low speed DIH, the volumetric PDF calculations were multiplied by a mean velocity factor from the curve fit function. Smaller particles had a larger velocity weighting factor due to higher mean velocities. This effect can be seen in the top row of Fig. 11. Low-speed DIH would not be imaging these particles with as much frequency as high speed DIH due to the low repetition rate when compared to the ejected velocity of the particles. Assuming conservation of mass and momentum, the ejected velocity of particles should be close to the burning rate. Burning rate calculations and measurements for these propellant formulations have been performed before [6]. Using the model developed for burning rate, with the appropriate parameters for both flake Al and spherical baseline, the burning rates are calculated as ~2 mm/s at 1 atmosphere. Comparing this burning rate to the frame difference for low-speed DIH, and combined with the pixel pitch of low-speed DIH, both

materials burn at ~3 mm/s, roughly the same value. High-speed DIH analysis report velocities of ejected droplets to be much greater by a few orders of magnitude in the meters per second range. A large quantity of smaller agglomerates could have been missed using low-speed DIH. Cumulative distribution functions (CDF) are compared from the raw low-speed, high-speed, and renormalized low-speed DIH data to illustrate the effect of the size velocity correlations. Both the size velocity correlations and CDF for baseline and flake Al can be seen in Fig. 11. The correction for baseline Al shifts the low speed data towards the high speed data, while the correction for the flake Al appears to over-correct the data, shifting the sizes towards smaller diameters than those sized from high-speed DIH.

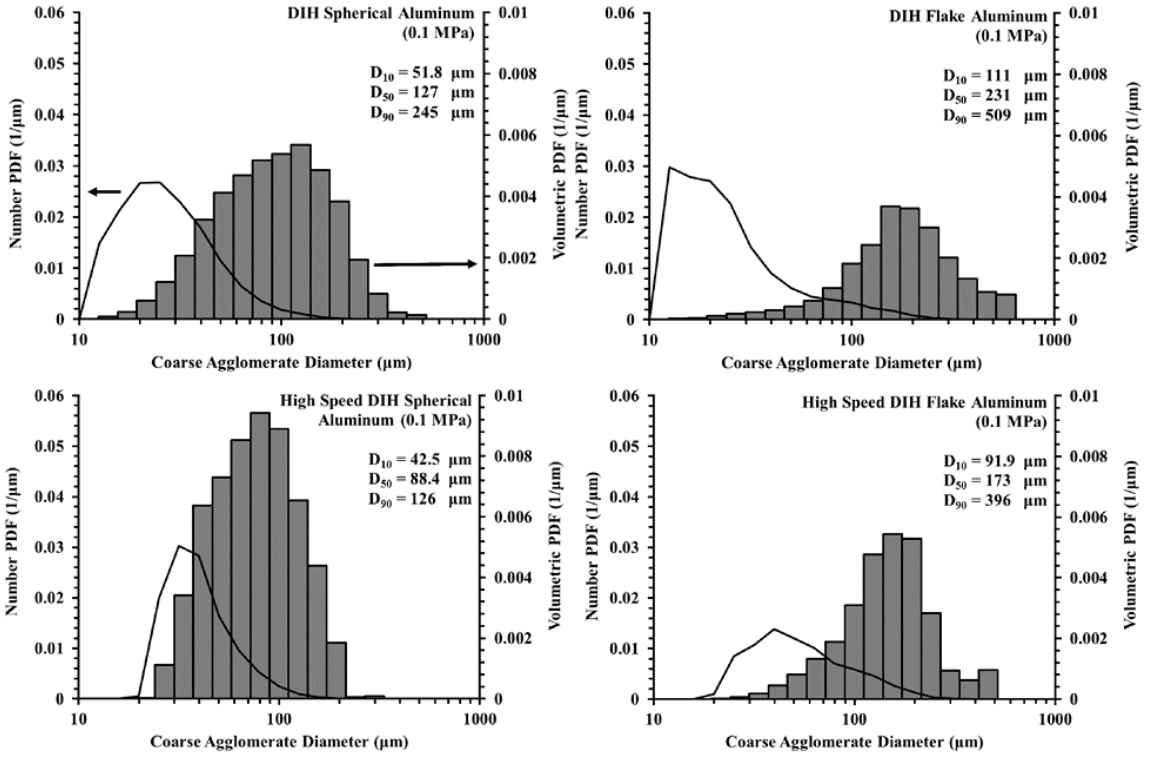

Fig. 10. From left to right shows spherical and flake Al additives for size comparisons, while the top row shows results from low-speed DIH and bottom row from high-speed DIH. Number PDF are shown as lines and volumetric PDF are shown as shaded rectangles.

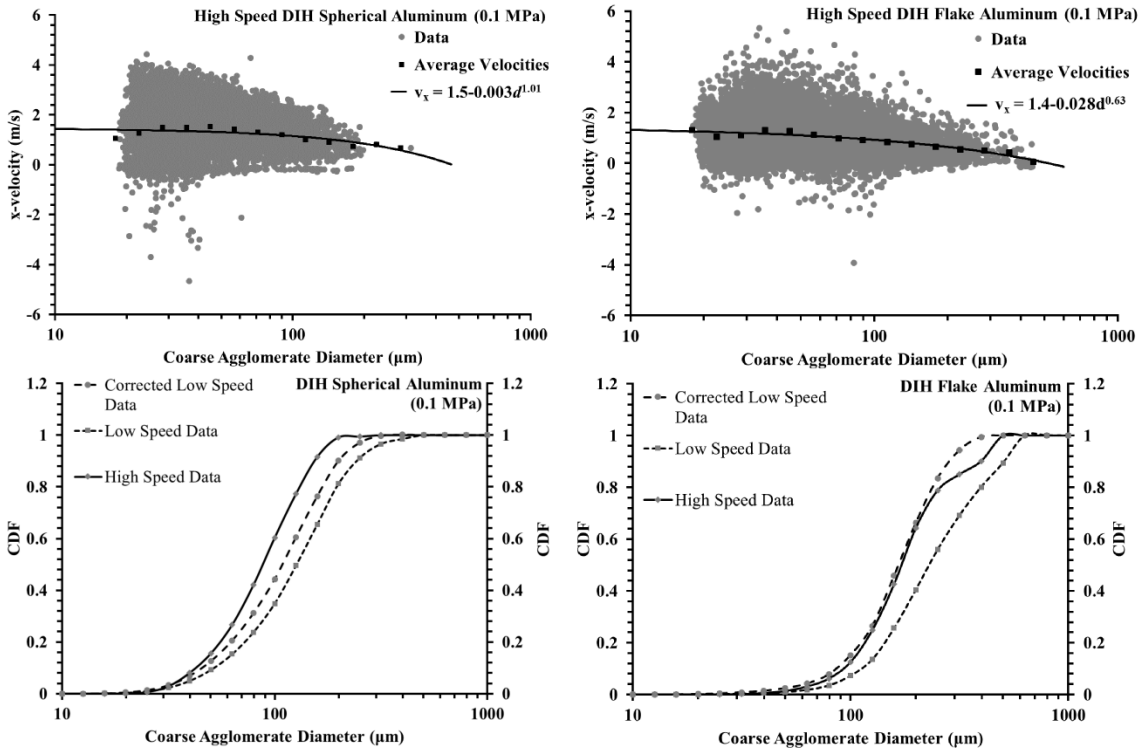

Fig. 11. Left column is spherical Al, and right column is flake Al. The top row is the raw data from size and velocity correlation, while the bottom row is CDF for high-speed, low-speed, and corrected low-speed DIH based on the weighting factors from the velocity fit functions in the top row. Data was fit based on mean velocities. The corrected data is in the middle for baseline, but appears to over-compensate for flake Al.

Particle collection is difficult overall in terms of experimental apparatus, microscope imaging, and image analysis. A difficulty of the analysis of samples from particle collection was highly dependent on the clarity of the contrast between the quench disk and the particles. Alumina smoke and other combustion products can condense onto the quench disk, as noticed by white outlines around particles, and can interfere in particle recognition for sizing agglomerates. This can be avoided based on the height of the quench plate and its velocity. Careful automated recognition of particles must be performed to get accuracy and repeatability when performing the microscopy and contrast imaging. Another problem with particle collection is that it cannot be used to record alumina smoke and burning

surface phenomena. Ideally, the best use for particle collection is for measurements at high pressure, where light and laser based techniques are more difficult to perform.

Imaging of particles from videography is somewhat similar to particle collection as particles were contrasted against an illuminated background. This technique is subject to any imaging flaws. Post-processing can eliminate this to some extent. Apparatus for this technique is the simplest of the three, allowing for rapid set up and testing of the experiment. Particles are counted every 10 frames to ensure particles do not get counted multiple times, and then sized based on detection in the image. Based on the velocities reported via high-speed DIH, particles will be out of frame after ~5 frames based on particles moving at the lowest reported velocities and the size of the imaging window. Using every 10 frames for the recorded media leads to approximately 750 usable frames per experiment. Combining the usable frame quantity and automated particle recognition issue, many particles are not counted and more experiments have to be performed to have a similar amount of particles for analysis as with low-speed DIH or particle collection. More material will need to be used to size agglomerates using this technique, which is problematic if the formulation is in limited quantities. LMD diameters are found to closer to high-speed DIH than low-speed DIH due to sampling bias towards larger particles for the latter. Unlike particle collection, flame phenomena (via alumina smoke) can be recorded in-situ during experiments. However, this method cannot be used for high pressure experiments that produce optically dense plumes that block most of the light. Furthermore, much higher regression rates of the propellants and particle velocities causes image blurring.

DIH is similar to videography for observing gas phase, surface, and flame phenomena. Using DIH results in much larger particle data sets in one experiment than with videography, by almost a factor of 10, because of the focal volume utilized in this technique. Many more particles can be analyzed from a single hologram in an experiment yielding better statistics and multiple holograms per experiment are possible with high-speed DIH. This is beneficial when very limited quantities of materials are available for testing or repeated testing is prohibitive. Preparation of experimental apparatus is relatively simple. The largest difficulty in this technique comes from the computational expense. Automated codes for DIH have to recreate different focal planes, size particles that are in focus, and repeat the procedure for each image recorded. This can become very computationally intensive, when there is a large amount of images, particularly for the case of high speed DIH. DIH can possibly be employed for high pressure experiments that form optically dense plumes, using different laser wavelengths that have high transmission. Low-speed DIH also does not suffer from motion blurring effects, because the q-switched laser used have pulse lengths shorter than 10 ns.

4 CONCLUSIONS

All methods demonstrated show similar trends in sizes for agglomerates with a majority of the mass being greater than the initial constituent particles. This agreement in sizing between all three techniques qualifies that any of the selected techniques could be used for imaging particles for accurately characterizing LMD sizes. Benefits and drawbacks exist for each technique. Particle collection in experimental set up and analysis is more difficult. This technique relies greatly on careful imaging and apparatus adjustments to get usable quenched LMD for analysis. It is also intrusive and particle splatter effects can bias the size distributions towards larger sizes. However, at high pressures where the optical density of the plume is very high, it produces more reliable results. Videography is favorable for initial sizing measurements compared to particle collection as the particle size analysis is automated. Apparatus involved with this technique is also simple when compared to particle collection. Videography is hindered by the number of experiments that must be performed to get the quantities of data available to the other techniques compared here. Videography also requires careful image brightness and contrast adjustment for accurate automated edge detection. DIH has the benefit of being easy to set up and a large quantity of LMD characterized per experiment. The difficulty in DIH comes from the computational expense required to size agglomerates. Focal planes, particles, and multiple videos must be analyzed which can be time consuming. Little oversight is required for this technique and material usage is minimized.

Size and velocities have been shown to have an impact on measurements for low speed compared to high-speed DIH, as larger particles have a smaller axial velocity leading to possible multiple counting of larger particles for low-speed DIH. This effect is not an issue for videography as even with the lowest reported velocity from high-speed DIH results, the difference in images used for sizing was at least 4 times larger than needed. The effect of particle velocity on low-speed DIH results for volumetric PDF shifts the PDF towards larger diameters. Velocity bias correction factors were implemented in order to reduce the effect of counting larger particles more frequently. Low speed baseline Al DIH data could be renormalized to improve the agreement with high-speed DIH and videography data. Flake Al low-speed DIH data correction initially showed good overlap with smaller diameters, but over-corrected the particle sizes to smaller particle sizes than measured with the high-speed DIH technique. Finding a better curve fit for the velocity correlations can result in better refinement of the data towards high-speed DIH.

5 FUTURE WORK

These techniques could be applied to sizing particles of modifying additives for APCP. This is inclusive, but not limited to, mechanically activated alloys, binary alloys, or nitramines. Mechanically activated and binary alloys alter the burning of characteristics of aluminum particles, possibly toward smaller agglomerates which may reduce two phase flow losses. Addition of nitramines would be a replacement for coarse AP for a more energetic additive for rocket motors, and possible reduction in hydrochloric acid.

Further characterization of the high speed DIH technique should also be performed. There is a size to velocity bias that exists with the low speed technique that favors slightly larger particles due to the extensive field of view used in the technique. Supplementary data should be analyzed to establish a better curve fit for correction of LMD sizes for low speed DIH data. This would allow for a more accurate representation of agglomeration reduction for new formulations, while minimizing material usage.

A future endeavor would be to apply the DIH technique to high pressure applications. Optical based techniques have seen little usage in high pressure applications due to opacity of the flow field. This is usually the case with larger samples. DIH requires minimal material for characterization of particle sizes. Smaller test samples could be utilized to offset this problem. Furthermore, the accuracy of the DIH technique is

influenced by the wavelength of the laser used. UV laser radiation could be used to offset the thick optical density plume from an aluminized propellant.

LIST OF REFERENCES

LIST OF REFERENCES

[1] P. Bucher, L. Ernst and F. L. Dryer, "Detailed Studies on the Flame Structure of Aluminum Particle Combustion," *AIAA,* vol. 185, pp. 689-722, 2000.

[2] E. W. Price, "Experimental solid rocket combustion instability," *Symposium (International) on Combustion,* vol. 10, no. 1, pp. 1067-1082, 1965.

[3] M. W. Beckstead, "A Summary of Aluminum Combustion," NATO RTO, Rhode-Saint-Genese, 2004.

[4] E. W. Price and R. K. Sigman, "Combustion of Aluminized Solid Propellants," *AIAA,* pp. 663-687, 1999.

[5] R. W. Hermsen, "Aluminum Combustion Efficiency," in *AIAA-81-0038,* St. Louis, 1999.

[6] T. R. Sippel, S. F. Son and L. J. Groven, "Aluminum agglomeration reduction in a composite propellant using tailored Al/PTFE particles," *Combustion and Flame,* vol. 161, no. 1, pp. 311-321, 2013.

[7] H. Cheung and N. S. Cohen, "Performance of Solid Propellants Containing Metal Additives," *AIAA,* vol. 3, no. 2, pp. 250-257, 1964.

[8] F. Maggi, A. Bandera, L. Galfetti, L. T. De Luca and T. L. Jackson, "Efficient solid rocket propulsion for access to space," *Acta Astronautica,* vol. 66, pp. 1563-1573, 2009.

[9] V. Babuk, I. Dolotkazin, A. Gamsov, A. Glebov, L. T. DeLuca and L. Galfetti, "Nanoaluminum as a Solid Propellant Fuel," *Fournal of Propulsion and Power,* vol. 25, no. 2, pp. 482-489, 2009.

[10] K. Jayaraman, S. R. Chakravarthy and R. Sarathi, "Quench collection of nano-aluminium agglomerates from combustion of sandwiches and propellants," *Proceedings of the Combustion Institute,* vol. 33, no. 2, pp. 1941-1947, 2011.

[11] L. Galfetti, L. T. DeLuca, F. Severini, G. Colombo, L. Meda and G. Marra, "Pre and post-burning analysis of nano-aluminized solid rocket propellants," *Aerospace Science and Technology,* vol. 11, no. 1, pp. 26-32, 2007.

[12] R. A. Yetter, G. A. Risha and S. F. Son, "Metal particle combustion and nanotechnology," *Proceedings of the Combustion Institue,* vol. 32, no. 2, pp. 1819-1838, 2009.

[13] T. R. Sippel, S. F. Son, L. J. Groven, S. Zhang and E. L. Dreizin, "Exploring mechanisms for agglomerate reduction in composite solid propellants with polyethylene inclusion modified aluminum," *Combustion and Flame,* 2014.

[14] R. Geisler, "A Global View of the Use of Aluminum Fuel in Solid Rocket Motors," in *38th AIAA/ASME/SAE/ASEE Joint Propulsion conference & Exhibit,* Indianapolis, Indiana, 2002.

[15] L. A. Povinelli and R. A. Rosenstein, "Alumina Size Distributions from High-Pressure Composite Solid-Propellant Combustion," *AIAA,* vol. 2, no. 10, pp. 1754-1760, 1964.

[16] H. L. Churchill, R. W. Fleming and N. S. Cohen, "Aluminum Behavior in Solid Propellant Combustion," AFRPL TR-74-12, May 1974.

[17] J. K. Sambamurthi, E. W. Price and R. K. Sigman, "Aluminum Agglomeration in Solid-Propellant Combustion," *AIAA Journal,* vol. 22, no. 8, pp. 1132-1138, 1984.

[18] D. Laredo and D. W. Netzer, "Application of Optical diagnostics to particle measurements in solid propellant rocket motors and exhaust plumes," *Particulate Science and Technology,* vol. 11, pp. 175-192, 1993.

[19] D. Laredo, J. I. McCrorie, J. K. Vaughn and D. W. Netzer, "Motor and plume particle size measurements in solid propellant micrometers," *Journal of Propulsion and Power,* vol. 10, no. 3, pp. 410-418, 1994.

[20] V. V. Karasev, A. A. Onischuk, O. G. Glotov, A. M. Baklanov, A. G. Maryasov, V. E. Zarko, V. N. Panfilov, A. I. Levykin and K. K. Sabelfeld, "Formation of charged aggregates of Al2O3 nanoparticles by combustion of aluminum droplets in air," *Combustion and Flame,* vol. 138, pp. 40-54, 2004.

[21] F. Cauty, C. Erades and J. M. Desse, "Light deviation based optical techniques applied to solid propellant combustion," *Progress in Propulsion Physics,* vol. 2, pp. 121-134, 2011.

[22] J. P. Powers and D. W. Netzer, "Automatic particles sizing from rocket motor holograms," in *SPIE Proceedings*, San Jose, CA, May 1992.

[23] J. D. Walker and D. W. Netzer, "Holographic Investigation of Metallized Solid Propellant Combustion in Two-Dimensional and Three-Dimensional Rocket Motors," Naval Postgraduate School, Monterey CA, 1987.

[24] A. G. Butler and D. W. Netzer, "Holographic Investigation of Solid Propellant Combustion," Naval Postgraduate School, Monterey, CA, 1988.

[25] D. E. Faber and D. W. Netzer, "Holographic Investigation of Solid Propellant Combustion Particulates," Naval Postgraduate School, Monterey, CA, 1983.

[26] D. R. Guildenbecher, M. A. Cooper, W. Gill, H. L. Stauffacher, M. S. Oliver and T. W. Grasser, "Quantitative, three-dimensional imaging of aluminum drop combustion in solid propellant plumes via digital in-line holography," *Optics Letters*, vol. 39, no. 17, pp. 5126-5129, 2014.

[27] J. C. Melcher, H. Krier and R. L. Burton, "Burning Aluminum Particles Inside a Laboratory-Scale Solid Rocket Motor," *Journal of Propulsion and Power,* vol. 18, no. 3, pp. 631-640, 2002.

[28] S. Goroshin, J. Mamen, A. Higgins, T. Bazyn, N. Glumac and H. Krier, "Emission spectroscopy of flame fronts in aluminum suspensions," *Proceedings of the Combustion Institute,* vol. 31, no. 2, pp. 2011-2019, 2007.

[29] J. Harrison and Q. Brewster, "Infrared Emitted Intensity Measurements from Burning Aluminum Droplets in Solid Propellants," *Combustion Science and Technology,* vol. 181, no. 1, pp. 18-35, 2008.

[30] T. R. Sippel, S. F. Son and L. J. Groven, "Altering Reactivity of Aluminum with Selective Inclusion of Polytetrafluoroethylene through Mechanical Activation," *Propellants, Explosives, Pyrotechnics,* vol. 38, pp. 286-295, 2013.

[31] D. Gabor, "Holography, 1948-1971," *Proceedings of the IEEE,* vol. 60, no. 6, pp. 655-668, 1972.

[32] U. Schnars and W. Jueptner, Digital Holography Digital Hologram Recording, NUmberical Reconstruction, and Related Techniques, Heidelberg: Springer, 2005.

[33] D. R. Guildenbecher, J. Gao, P. L. Reu and J. Chen, "Digital holography simulations and experiments to quatify the accuracy of 3D particle location and 2D sizing using a proposed hybrid method," *Applied Optics,* vol. 52, no. 16, pp. 3790-3801, 2013.

[34] F. L. Pedrotti, L. S. Pedrotti and L. M. Pedrotti, Introduction to Optics, New Jersey: Prentice Hall, 2007.

[35] J. W. Goodman, Introduction to Fourier Optics, McGraw Hill, 1996.

[36] D. R. Guildenbecher, J. Gao, P. L. Reu and J. Chen, "Digital holography simulations and experiments to quantify the accuracy of 3D particle location and 2D sizing using a proposed hybrid method," *Applied Optics,* vol. 52, no. 16, pp. 3790-3801, 2013.